TSG101 negatively regulates mitochondrial biogenesis in axons

Tzu-Huai Lin[a], Dana M. Bis-Brewer[b,c], Amy E. Sheehan[a], Louise N. Townsend[d], Daniel C. Maddison[e], Stephan Züchner[b,c], Gaynor A. Smith[e,1], and Marc R. Freeman[a,1]

[a]Vollum Institute, Oregon Health & Science University, Portland, OR 97239; [b]John P. Hussman Institute for Human Genomics, University of Miami, Miami, FL 33136; [c]Dr. John T. Macdonald Foundation Department of Human Genetics, University of Miami, Miami, FL 33136; [d]UK Dementia Research Institute, School of Biosciences, Cardiff University, Cardiff CF24 4HQ, United Kingdom; and [e]UK Dementia Research Institute, School of Medicine, Cardiff University, Cardiff CF24 4HQ, United Kingdom

Edited by Liqun Luo, Stanford University, Stanford, CA, and approved April 5, 2021 (received for review September 6, 2020)

There is a tight association between mitochondrial dysfunction and neurodegenerative diseases and axons that are particularly vulnerable to degeneration, but how mitochondria are maintained in axons to support their physiology remains poorly defined. In an in vivo forward genetic screen for mutants altering axonal mitochondria, we identified *tsg101*. Neurons mutant for *tsg101* exhibited an increase in mitochondrial number and decrease in mitochondrial size. TSG101 is best known as a component of the endosomal sorting complexes required for transport (ESCRT) complexes; however, loss of most other ESCRT components did not affect mitochondrial numbers or size, suggesting TSG101 regulates mitochondrial biology in a noncanonical, ESCRT-independent manner. The TSG101-mutant phenotype was not caused by lack of mitophagy, and we found that autophagy blockade was detrimental only to the mitochondria in the cell bodies, arguing mitophagy and autophagy are dispensable for the regulation of mitochondria number in axons. Interestingly, TSG101 mitochondrial phenotypes were instead caused by activation of PGC-1α/Nrf2-dependent mitochondrial biogenesis, which was mTOR independent and TFEB dependent and required the mitochondrial fission–fusion machinery. Our work identifies a role for TSG101 in inhibiting mitochondrial biogenesis, which is essential for the maintenance of mitochondrial numbers and sizes, in the axonal compartment.

mitochondria | mitochondrial biogenesis | ESCRT | TSG101 | neurodegeneration

Mitochondria are vital organelles for all cells, but the highly polarized architecture of neurons presents a unique challenge in distributing these organelles to support cellular physiology. Axons in particular, which can be extremely long, must be supported at great distances from the cell bodies. How mitochondrial populations in axons are established and maintained at the correct density and distribution is not understood, but it is clear that axons lacking mitochondria can exhibit blocked growth or frank degeneration (1, 2). Alterations in mitochondrial function are tightly associated with nearly all neurodegenerative diseases, and axons, perhaps due to their enormous size, seem to be particularly vulnerable to degeneration (3–6). Unraveling the mechanisms by which axons receive and maintain appropriate numbers of healthy mitochondria is of paramount importance to defining the basic cell biological principles of axonal maintenance, and it is likely that such insights will shed light on mechanisms that drive neurodegeneration.

Mitochondria are intricately linked to many cellular functions. It is important to keep a constant functional pool of mitochondria through the generation of new mitochondria and eliminating malfunctioning ones. Mitochondria undergo fission to produce new mitochondria from existing ones, and the master transcriptional coactivator PPAR gamma coactivator, PGC-1α, is required to express nuclear-encoded mitochondrial genes to supply newly generated mitochondria with the molecules essential for function (7). When mitochondria are dysfunctional and need to be turned over, Pink1 can accumulate on mitochondria in response to a loss of mitochondrial membrane potential, where it recruits Parkin to initiate mitophagy or mitochondrial autophagy, whereby Parkin ubiquitinates proteins on the mitochondrial surface in order for autophagy machinery to recognize the doomed mitochondrion and target it for degradation (8–13).

While Pink1/Parkin-mediated mitophagy has been considered a major mechanism for disposing of mitochondria, recent studies have revealed a link between the endosomal sorting complexes required for transport (ESCRT) machinery and mitochondrial clearance. CHMP2A/Vps2 in the ESCRT-III complex is required during mitophagy for phagophore closure to form functional autophagosomes (14, 15). Snf8/Lsn in the ESCRT-II and TSG101 in the ESCRT-I complexes are involved in autophagy-independent but Parkin-dependent mitochondrial clearance (16). How and whether ESCRT complexes might regulate mitochondrial clearance in vivo has not been explored nor have roles for ESCRT complexes in mitochondrial biogenesis.

Despite our growing understanding of molecules regulating mitochondrial biology, the mechanisms by which cells maintain a properly sized, functional pool of mitochondria in vivo remain enigmatic. Given that many molecules known to regulate mitochondria

Significance

Mitochondrial dysfunction has been associated with many age-dependent neurodegenerative disorders such as Parkinson's and Alzheimer's disease, yet understanding how a neuron maintains a pool of functional mitochondria in sufficient density and location throughout axons in vivo still remains enigmatic. Through an unbiased in vivo forward genetic screen, we identified an endosomal sorting complexes required for transport component, TSG101, as a modulator of mitochondrial number and size in neurons and provide evidence to place TSG101 as a negative regulator of mitochondrial biogenesis. We further find that TSG101 does not contribute to Parkin/Pink1-mediated mitophagy and discovered that macroautophagy regulators ATG1 and ATG6 are dispensable in axonal mitochondrial number regulation. Through in vivo screening, it is possible to unravel translatable mechanisms of axonal mitochondrial maintenance.

Author contributions: T.-H.L., G.A.S., and M.R.F. designed research; T.-H.L., D.M.B.-B., L.N.T., D.C.M., S.Z., and G.A.S. performed research; A.E.S. contributed new reagents/analytic tools; T.-H.L., D.M.B.-B., S.Z., and G.A.S. analyzed data; and T.-H.L., G.A.S., and M.R.F. wrote the paper.

The authors declare no competing interest.

This article is a PNAS Direct Submission.

[1]To whom correspondence may be addressed. Email: smithga@cardiff.ac.uk or freemmar@ohsu.edu.

This article contains supporting information online at https://www.pnas.org/lookup/suppl/doi:10.1073/pnas.2018770118/-/DCSupplemental.

Published May 10, 2021.

were discovered in nonneuronal cells in an in vitro setting, determining how these mechanisms translate into in vivo mitochondrial regulation is also an important and often outstanding question. Hence, we performed an in vivo forward genetic screen in *Drosophila* (17) for mutations that exhibited changes in axonal mitochondrial size, number, or distribution. After screening over 6,000 genomes, we identified TSG101 as a regulator of axonal mitochondria. *tsg101* mutants exhibited elevated mitochondrial

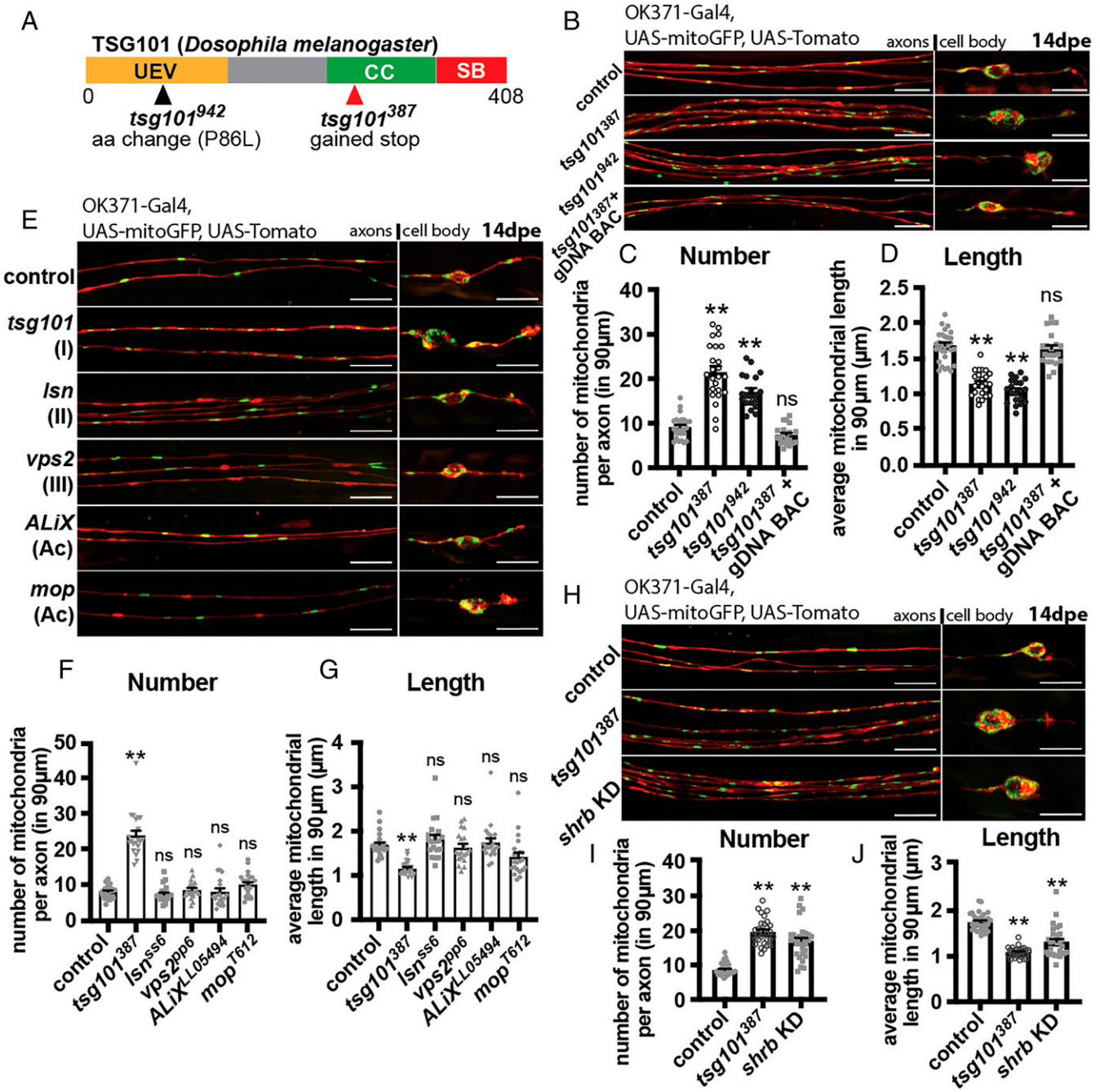

Fig. 1. TSG101 functions as a regulator of axonal mitochondria in a noncanonical ESCRT manner. Homozygous mutant glutamatergic neurons were generated in *Drosophila* wings using the MARCM approach, where the mutants were fluorescently labeled with myr::td-Tomoato (red) and mito::EGFP (green). The flies were grown at 25 °C, and the cell bodies and the axons of the neurons were examined by fluorescence microscopy at 14 dpe. (*A*) Diagram of the nature of different *tsg101* alleles. $tsg101^{387}$ was the allele identified in the screen, which contains a premature stop in the coiled-coil domain (CC) (red arrowhead). $tsg101^{942}$ is a publicly available null allele that has an amino acid change in the Ubiquitin E2 variant domain (UEV) (black arrowhead). (*B–D*) Both of the alleles of TSG101 exhibited increased mitochondrial number and decreased mitochondrial size, and this phenotype could be rescued by reexpressing TSG101 using genomic DNA BAC. At least 20 wings (one wing/animal) were examined for each genotype ($n \geq 20$). Every individual data point represents one animal. (*E*) Null alleles of each gene in different ESCRT complexes were selected to generate homozygous mutant clones in *Drosophila* wings: $tsg101^{387}$ in the ESCRT-I (I), lsn^{ss6} in the ESCRT-II (II), $vps2^{pp6}$ in the ESCRT-III (III), and $ALiX^{LL05494}$ and mop^{T612} in the accessory complex (Ac). Mitochondrial (*F*) number and (*G*) length were analyzed and quantified. (*H–J*) Knockdown of *shrb* (*shrb* KD, RNAi line BDSC:38305) of the ESCRT-III showed *tsg101*-mutant–like phenotype. $n \geq 30$. All data were analyzed via one-way ANOVA. $^{**}P < 0.01$ and ns: not significant. Error bar: SEM. (Scale bar, 10 μm.)

numbers and reduced mitochondrial length. TSG101 is a component of the ESCRT-I complex; however, other key components of the ESCRT complexes were not required for normal axonal mitochondrial number or size, suggesting TSG101 functions in this context in a noncanonical way. Blocking either Pink1/Parkin-mediated mitophagy or macroautophagy exerted no significant effect on axonal mitochondrial morphology, suggesting mitophagy/autophagy are also dispensable in the axons. Instead, TSG101 loss activated mitochondrial biogenesis in an mTOR-independent and TFEB-dependent manner, to increase number and reduce the size of mitochondria. Our work argues that TSG101 is a critical regulator of axonal mitochondrial populations and that canonical

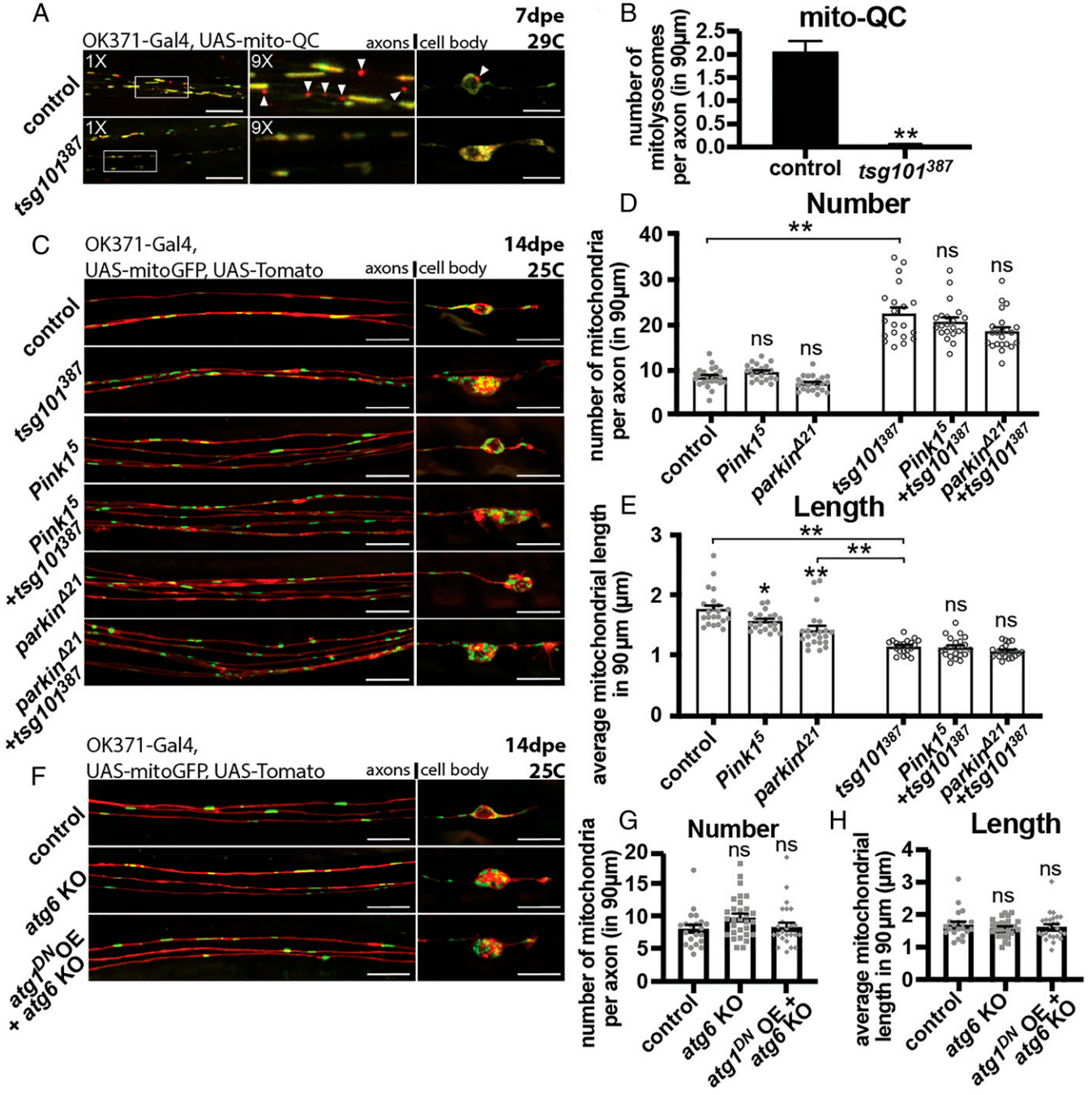

Fig. 2. Blocking mitophagy/autophagy in neurons did not recapitulate the axonal mitochondrial phenotype of *tsg101* mutants. (*A* and *B*) Mito-QC was utilized to visualize mitochondrial turnover event: normal mitochondria in yellow (green + red) and lysosome-associated mitochondria in red (mitolysosomes, indicated by white arrowheads). Flies were grown in 29 °C and checked at 7 dpe. Number of mitolysosomes per axon in *A* was quantified and shown in *B*, analyzed by unpaired *t* test. $n = 10$. (*C–E*) Homozygous mutant neurons were sparsely generated and labeled red and mitochondria in green. Null alleles of *Pink1* (*Pink1*^{5}) and *parkin* (*parkin*$^{\Delta 21}$) were used to suppress mitophagy. Flies were grown in 25 °C and checked at 14 dpe. Mitochondria were subsequently quantified and analyzed in *D* and *E*. $n \geq 20$. Data were analyzed via two-way ANOVA. $^{*}P < 0.05$. $^{**}P < 0.01$. (*F–H*) Blocking autophagy by knocking out *atg6* (Beclin-1) and/or overexpressing dominant-negative *atg1* (ULK1). Flies were grown in 25 °C and checked at 14 dpe. Quantification of axonal mitochondria is shown in *G* and *H*; analyzed via one-way ANOVA. $n \geq 20$. Error bar: SEM. (Scale bar, 10 µm.)

Pink1/Parkin and autophagy-dependent mechanisms for mitochondrial turnover do not predominate in the axonal compartment.

Results

***tsg101* Mutants Exhibited Increased Mitochondrial Number and Decreased Mitochondrial Size in Axons.** To identify genes involved in the maintenance of axonal mitochondria in vivo, we performed a forward genetic screen for mutants with altered mitochondria in the axons of adult *Drosophila* L1 wing-vein glutamatergic sensory neurons (17). We mutagenized animals with ethyl methanesulfonate (EMS) and used an F_1 mosaic analysis with a repressible cell marker (MARCM)-based genetic approach (18) to generate sparse, homozygous mutant clones, where the plasma membrane was labeled with td-Tomato (myr::td-Tomato) and mitochondria with GFP (mito::EGFP). Potential mitochondrial regulating molecules were indicted based on changes in mitochondrial morphology and number or distribution in either the axon and/or cell body, with the preliminary screen identifying five candidates, including one previously mapped and characterized regulator *gfzf* (17). We quantified mitochondrial populations 1, 7, and 14 d posteclosion (dpe) in individual axons and bred F_1 animals with altered mitochondrial profiles. We identified one mutant, *l(3)387*, that bred true and was subsequently named $tsg101^{387}$ after rigorous tests, including complementation test (*SI Appendix*, Fig. S1*A*) and next-generation whole-genome sequencing that identified a gained stop in the gene *tsg101* as the causal lesion (Fig. 1*A*). Mutations in the gene caused early larval lethality and hence phenotypes were studied in neuronal clones. $tsg101^{387}$ mutants exhibited elevated mitochondrial number and shortened mitochondrial length. At 14 dpe, while control animals averaged below 10 mitochondria (per 90 μM of axon scored), $tsg101^{387}$ mutant axons had more than 21 mitochondria in the same area of axon, although they were reduced in size by over 30% (Fig. 1 *B–D*), resulting in an increase in overall axonal occupation by mitochondria (*SI Appendix*, Fig. S1*B*). This change in mitochondrial morphology manifested as early as 1 dpe, and the phenotypical differences widened as the time elapsed (*SI Appendix*, Fig. S1 *D–F*). In addition to the mitochondrial phenotype, we also observed a neuronal phenotype, in which the cell bodies of the mutant neurons were consistently larger than the control (*SI Appendix*, Fig. S1*F*), and at 30 dpe neurons underwent spontaneous neurodegeneration (*SI Appendix*, Fig. S1*C*). Next, we determined the localization of TSG101 using antibody detection in primary mouse neurons. TSG101 was ubiquitously expressed, partly colocalizing with both mitochondria and endosomes in projections (*SI Appendix*, Fig. S1 *G* and *H*). Lastly, we a found a dramatic increase in endolysosomes in both the axons and the cell bodies of the mutant neurons, and the mutant axons exhibited more stationary endolysosomes in close proximity to the mitochondria than the control did (*SI Appendix*, Fig. S2), indicating the importance of TSG101 for mitochondrial maintenance, neuronal integrity, and endolysosomal homeostasis.

TSG101 and Shrb, but Not Other ESCRT Complex Components, Regulate Axonal Mitochondria and Axon Integrity. TSG101 is best known as a component of the ESCRT-I complex, one of several ESCRT complexes (ESCRT-I, ESCRT-II, ESCRT-III, and the accessory ESCRT complex) that drive the functional maturation of endosomes into multivesicular bodies. To determine whether other ESCRT-associated molecules also regulate axonal mitochondria, we knocked down most components of all ESCRT complexes by RNA interference (RNAi). To our surprise, knockdown of core ESCRT pathway components did not phenocopy the increased mitochondrial number and decreased mitochondrial length, as observed in the *tsg101* mutant, with the exception of *shrb-RNAi* (*SI Appendix*, Table S1). Shrb is a homolog of *vps32*/*snf7* in the ESCRT-III complex. Knockdown of *shrb* fully phenocopied mitochondrial phenotypes in *tsg101* loss-of-function mutants (Fig. 1 *H–J*). However, we were unable to generate clones for analysis of adult axons as *shrb* mutant glutamatergic neurons underwent cell death by 1 dpe. To further rule out a role for the major ESCRT complexes in regulation of axonal mitochondria, we used more rigorous loss-of-function genetic methods. We generated MARCM clones using tested and published null alleles of at least one component of each major ESCRT complex and found that knockout (KO) of *lsn* (ESCRT-II), *vps2* (ESCRT-III), or *ALiX* and *mop* (accessory complex) did not recapitulate the $tsg101^{387}$ mutant phenotype (Fig. 1 *E–G*). Together, these data support the notion that TSG101 does not regulate axonal mitochondria through canonical ESCRT signaling.

Turnover of Mitochondria in Axons Is Attenuated in *tsg101* Mutants, and the Turnover Does Not Require Parkin/Pink1-Mediated Mitophagy or Autophagy. The increase in mitochondrial number in axons that we observed in *tsg101* mutants might be the result of failed mitochondrial clearance or activated mitochondrial biogenesis. Given that some ESCRT complex components have recently been found to be required for mitochondrial clearance (14–16), we first assayed mitochondrial clearance. We used the well-established genetic tool mito-QC, which allows for monitoring of mitochondrial turnover induction using a pH-sensitive fluorophore, whose fluorescence is altered upon mitochondrial entry into acidic vesicles during degradation (Fig. 2*A*) (19, 20). In control animals, we observed normal (yellow) mitochondria, along with (red) mitolysosomes, which represent mitochondria undergoing lysosomal degradation, in both axons and the cell body. However, in $tsg101^{387}$ mutants, mitolysosomes were nearly undetectable (Fig. 2 *A* and *B*), indicating that mitochondrial turnover was largely attenuated. Live cell imaging revealed that lysosomes accumulated in axons, were more stationary, and were found in close proximity to mitochondria (*SI Appendix*, Fig. S2), indicating that loss of mitophagy may occur through defective mitolysosome trafficking.

To determine if loss of mitophagy could phenocopy the alterations in axonal mitochondria observed in *tsg101* mutants, we blocked mitophagy by knocking out Parkin or Pink1. We found that neither *parkin* nor Pink1 loss-of-function mutants phenocopied $tsg101^{387}$ mutants. We also found that neither mutant exerted significant effects on axonal mitochondrial numbers or size nor long-term axon maintenance (Fig. 2 *C–E*). We conclude that inhibition of Pink1/Parkin-mediated mitophagy does not explain the abnormal mitochondrial properties observed in the *tsg101* mutants. These data argue strongly that Pink1/Parkin-mediated mitophagy is not the primary mechanism for turnover of mitochondria in axons, and emerging evidence supports the notion that basal mitophagy can be Parkin and Pink1 independent (12, 19, 21).

We next blocked mitophagy via a more extreme means—impeding the entire autophagy process by knocking out *atg6* (Beclin-1 homolog) and/or overexpressing dominant-negative *atg1* (ULK1 homolog). *atg6* loss did not affect axonal mitochondria number or size nor did combining *atg6* loss with simultaneous expression of $atg1^{DN}$ (Fig. 2 *F–H*). However, we did observe that the cell bodies drastically increased in size (Fig. 2*F* and *SI Appendix*, Fig. S3*A*). Moreover, somal mitochondria changed from linear shapes to more globular ones (reflected in lower aspect ratio in $tsg101^{387}$ mutants; *SI Appendix*, Fig. S3*B*), and the mitochondrial mass significantly increased (*SI Appendix*, Fig. S3*C*), although the increase is proportionate to that in cell body size, leading to no change in overall mitochondrial coverage (*SI Appendix*, Fig. S3*D*). This phenotype persisted up to 30 dpe, where the cell body phenotype progressively worsened, while axonal mitochondria remained morphologically similar to wild type, although occasional axon blebs were apparent (*SI Appendix*, Fig. S3*E*). As we confirmed that mitochondria were no longer able to undergo mitophagy when autophagy is genetically blocked (*SI Appendix*, Fig. S3 *F* and *G*), we conclude that axonal mitochondrial populations can be maintained at normal levels even in the absence of Pink1, Parkin, or autophagy. This suggests that the

TSG101-mediated, autophagy-independent but Parkin-dependent mitochondrial clearance reported previously (16) is mechanistically distinct from TSG101-mediated mitochondrial clearance in axons. Furthermore, our data support the premise that mitochondrial clearance mechanisms are compartmentalized in neurons, since we observe changes in mitochondria in cell bodies with manipulation of autophagy but not in axons.

Mitochondria in *tsg101*-Mutant Neurons Have Lower Reactive Oxygen Species and Generate Increased Levels of ATP. TSG101 could be involved in mitochondrial clearance through a mechanism that does not require Pink1/Parkin or autophagy. If that is the case, we would predict that *tsg101*-mutant neurons would accumulate dysfunctional mitochondria and potentially have decreased ATP levels. To explore this possibility, we utilized two different roGFP genetic tools (GSSG-sensing and H_2O_2-sensing) to measure redox potential in mitochondria, which is an indicator of overall mitochondrial health—an increased oxidation state, which increases the 405/488-nm ratio, correlates well with increased mitochondrial damage and dysfunction (22). Interestingly, mitochondria in *tsg101*-mutant axons were less oxidized than in controls. As a further control for the sensors, we overexpressed human mitochondrial uncoupling protein (hUCP2), which artificially renders mitochondria more oxidized, and observed a >50% increase in the 405/488-nm ratio (Fig. 3 *A*–*D*). These data suggest that mitochondria in *tsg101* mutants were less oxidized and healthier than in controls. Moreover, when we utilized the ATP sensor ATPsnFR (23), we found that neurons lacking TSG101 had significant increased levels of cytoplasmic ATP, and this increase was abolished when oxidative phosphorylation (OXPHOS) was disrupted with hUCP2 overexpression (24), indicating that a lack of TSG101 results in more mitochondria synthesizing increased levels of axonal ATP (Fig. 3 *E* and *F*). These results suggest that the lack of mitochondrial turnover in *tsg101* mutants may be due to the fact that the mitochondria were hyperfunctional and thereby resistant to mitochondrial clearance.

Loss of TSG101 Activates Mitochondrial Biogenesis through PGC-1α, Nrf2, and TFEB. The majority of mitochondrial genes are encoded by the nuclear genome, and the master transcription coactivator PGC-1α and Nrf2 are responsible for activating nuclear-encoded mitochondrial gene expression. To investigate whether the hyperfunctional mitochondria in *tsg101* mutants were the result of activated mitochondrial biogenesis, we knocked down *srl* (the *Drosophila* PGC-1α homolog) and *cnc* (the *Drosophila* Nrf2 homolog) in both controls and *tsg101*-mutant neurons. Knockdown of *srl* or *cnc* in controls resulted in smaller mitochondria but normal numbers of mitochondria in the axon (Fig. 4 *A*–*C*). This is consistent with a decrease in overall mitochondrial content, which is expected after blocking mitochondrial biogenesis. When we knocked down *srl* or *cnc* in $tsg101^{387}$ mutants, the $tsg101^{387}$ mutant mitochondrial phenotypes were rescued, and this was true when we tested two different RNAi lines for *srl* and *cnc* (Fig. 4 *A*–*C*).

TFEB is a positive regulator of PGC-1α–mediated mitochondrial biogenesis during conditions such as nutrient deprivation and exercise (25, 26). We therefore investigated the role of TFEB as a potential activator of PGC-1α–mediated mitochondrial biogenesis in *tsg101*-mutant axons. Knockdown of *mitf* (the *Drosophila* TFEB homolog), with two independent RNAi lines, rescued *tsg101*-mutant mitochondrial phenotypes (Fig. 5 *A*–*C*), indicating that TFEB also acts downstream of TSG101 in controlling mitochondrial biogenesis. The mTOR pathway is also a modulator of mitochondrial biogenesis (7, 27) and can control TFEB activation (28, 29). Interestingly, a mutation in the gene encoding the mTOR inhibitor, Tsc1, was also uncovered in our forward genetic screen, with a phenotype of increased mitochondria numbers in axons; loss of *tsc1* has also been found to activate mitochondrial biogenesis (30). We therefore knocked down *tsc1* in control and *tsg101*-mutant clones and assayed mitochondrial phenotypes. We found that mitochondrial number was significantly increased after depletion of Tsc1, at levels even higher than in TSG101 mutants alone, although we detected no difference in mitochondrial size. In addition, we found that knockdown of Tsc1 in TSG101 null clones had no additive effect on the number of mitochondria in axons (*SI Appendix*, Fig. S4 *A*–*C*). This finding suggests that TSG101 controls mitochondrial biogenesis in an mTOR-independent manner or at least not through Tsc1. Therefore, our model suggests that TSG101 functions in a parallel pathway to mTOR, which converges on TFEB to regulate mitochondrial biogenesis.

Mitochondrial Biogenesis in *tsg101* Mutants Requires Drp1-Dependent Mitochondrial Fission. Mitochondria are generated by fission of existing mitochondria, which can be achieved by activating fission or inhibiting fusion. We first sought to determine whether the mitochondrial biogenesis activated in *tsg101* mutants required mitochondrial fission. We blocked fission by knocking out the critical fission gene *Drp1*, which significantly rescued both the mitochondrial number and size in axons caused by *tsg101* knockdown (*SI Appendix*, Fig. S5). This indicates that Drp1-mediated mitochondrial fission is downstream of TSG101 loss and is required for activation of mitochondrial biogenesis.

We next explored the effects of blocking mitochondrial fusion by knocking down the essential fusion gene Marf in attempt to recapitulate *tsg101*-mutant phenotype. Knockdown of Marf in control clones successfully shortened mitochondria to levels indistinguishable from $tsg101^{387}$ mutants at 7 dpe yet had no effect on number (*SI Appendix*, Fig. S6 *A*–*C*). To our surprise, Marf knockdown rescued mitochondrial number in *tsg101*-mutant axons to near control levels (*SI Appendix*, Fig. S6 *A* and *B*). We further investigated the effect of Marf knockdown at the earliest time point, 1 dpe, where the mitochondrial phenotype was not fully manifested and Marf knockdown had little effect (*SI Appendix*, Fig. S6 *D*–*F*). This suggests that the age-dependent increase of mitochondrial number from 1 to 7 d requires Marf, and fusion is a necessary initial step for biogenesis.

TSG101 Regulates Mitochondria and Neurodegeneration through Independent Pathways. Loss of TSG101 leads to spontaneous neurodegeneration in mutant clones as animals age (*SI Appendix*, Fig. S1*C*). We wished to determine whether this phenotype could also be rescued by manipulating mitochondrial biogenesis and to explore the molecular nature of the signaling pathways driving this axon degeneration. Given that knockdown of TFEB or Nrf2 rescued the defects in mitochondrial numbers and size in *tsg101* mutants, we explore whether these manipulations also prevented neurodegeneration. We found that knocking down TFEB (Mitf) or Nrf2 (Cnc) did not affect neurodegeneration nor axon survival rate, despite complete rescue of mitochondrial phenotypes (*SI Appendix*, Fig. S7 *A* and *B*). This argues strongly that TSG101 has two roles in axons, one to inhibit mitochondrial biogenesis and another to maintain long-term axon integrity. What is the nature of the neurodegeneration we observe? To explore this, we used a variety of manipulations to block Wallerian degeneration and apoptotic pathways using well-established genetic tools: Wld^{S}, $p53^{DN}$, or *p35* (31–33). Interestingly, neither blockade of Wallerian degeneration signaling (via Wld^{S} expression) or apoptosis signaling (via $p53^{DN}$ or *p35* expression) were able to suppress the neurodegeneration in *tsg101*-mutant clones (*SI Appendix*, Fig. S7*C*). These data argue that the neurodegeneration caused by lack of TSG101 occurs through mechanisms independent of canonical Wallerian degeneration and apoptotic signaling pathways.

Discussion

The remarkable size and morphological complexity of axons present an enormous challenge for neurons—how does the neuron establish and maintain a healthy population of mitochondria at

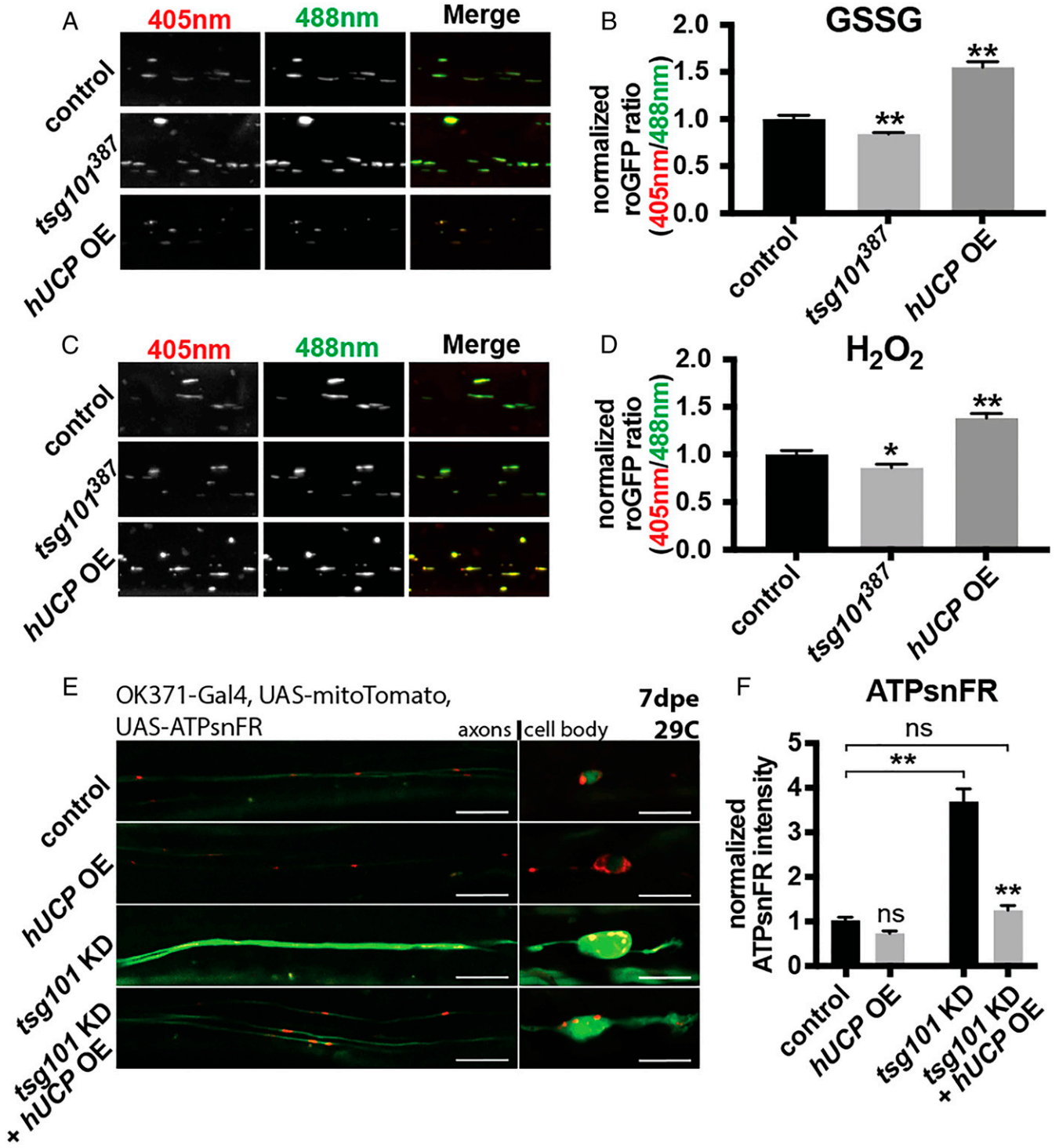

Fig. 3. Mitochondria in *tsg101* mutants were less oxidized and generated more ATP. (*A–D*) Redox-sensing GFPs (roGFPs) were utilized and expressed in mitochondria to reactive oxygen species. Fluorescence intensities were measured with 405-nm (pseudocolored red) and 488-nm (pseudocolored green) laser excitations. roGFP ratios were determined by the measured fluorescence intensity from 405 nm divided by that from 488 nm. 405/488-nm ratios were normalized to the control. A higher ratio indicates a more oxidized mitochondrion. Overexpression of human uncoupling protein (hUCP2) was used to make mitochondria more oxidized by disrupting mitochondrial membrane potential in order to reassure the reliability of the sensors. Flies were grown in 25 °C and checked at 14 dpe. Data were analyzed via unpaired *t* test. $n \geq 10$. Error bar: SEM. $^{*}P < 0.05$. $^{**}P < 0.01$. (*E* and *F*) ATP-sensing GFP (ATPsnFR, green) was expressed in the cytosol to measure cytosolic ATP level. ATPsnFR intensities were normalized to the fluorescence intensity of mitochondria (mito::td-Tomomato, red), and the normalized ATPsnFR intensities were then normalized again to that of control. Flies were raised in 29 °C and examined at 7 dpe. $n \geq 14$. Data were analyzed via two-way ANOVA. Error bar: SEM. (Scale bar, 10 μm.) $^{**}P < 0.01$.

sufficient density throughout their axonal arbors? This problem, termed neuronal mitostasis (34), is ongoing throughout the animal's lifespan and must be dealt with successfully in order to sustain the energetically expensive process of neurotransmission and to maintain neuronal integrity. Mitochondrial populations in axons are believed to be regulated primarily by mitochondrial

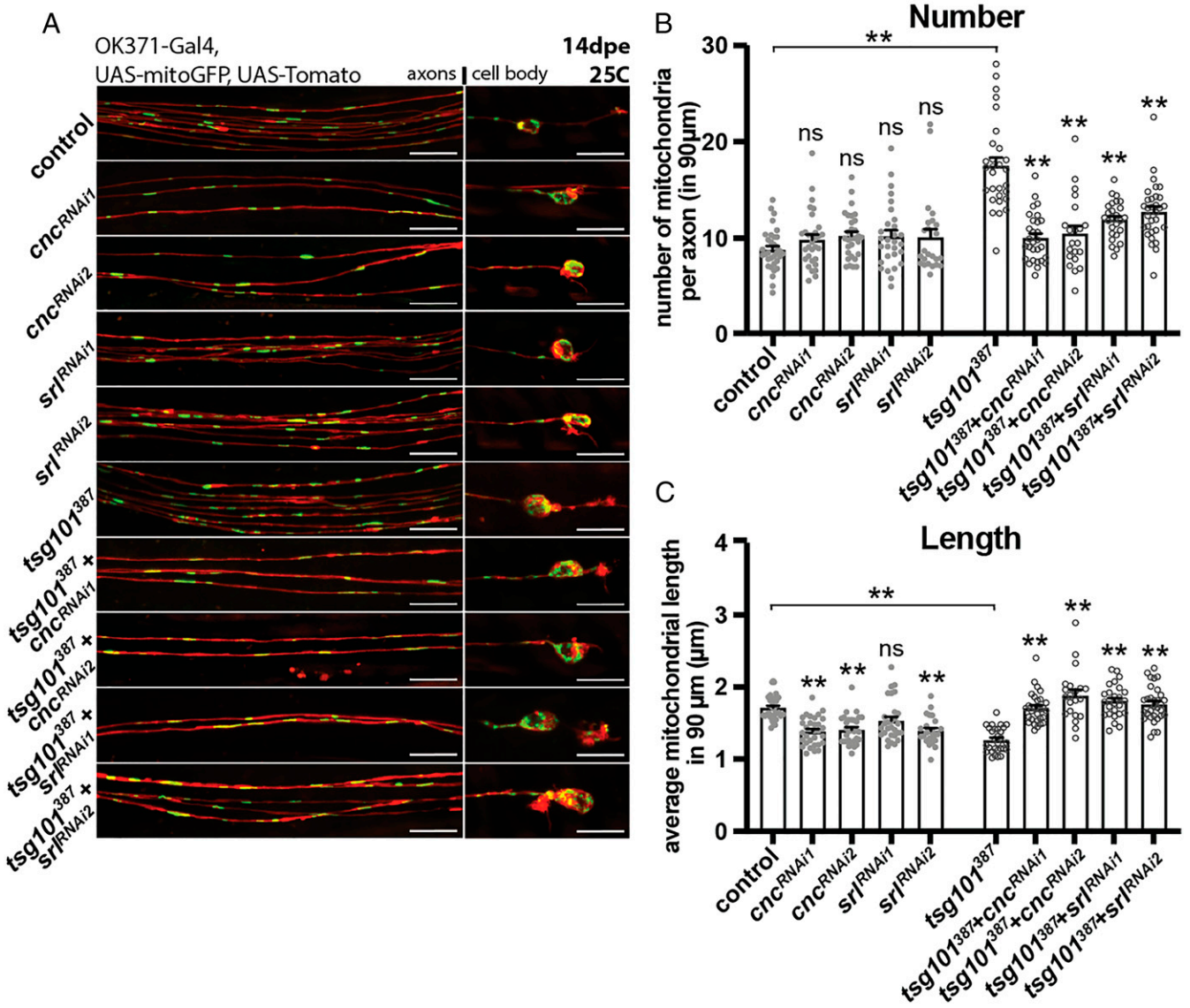

Fig. 4. Loss of TSG101 activates PGC-1α (*srl*)/Nrf2 (*cnc*)-dependent mitochondrial biogenesis. (*A*–*C*) Homozygous mutant neurons were generated and labeled using the same approach as in Fig. 1. Two independent RNAi were used to knock down PGC-1α (*srl*) or Nrf2 (*cnc*). All four independent RNAi were able to successfully rescue the mitochondrial phenotype resulted from TSG101 ablation. Quantification of (*B*) number and (*C*) length. $n \geq 30$. Data were analyzed via two-way ANOVA. Error bar: SEM. $^{**}P < 0.01$. (Scale bar, 10 μm.)

transport into the axon (i.e., motility), anchoring, and fission and fusion to increase or decrease numbers, respectively. Turnover of damaged mitochondria or their components is mediated by the shedding of mitochondria-derived vesicles (MDVs), which are used to degrade packages of lipids and proteins (35, 36), mitophagy, or the general cellular degradative macroautophagy pathway. The critical importance of neuronal mitostasis is borne out by the fact that mutations in many genes that regulate mitochondrial function (37) or dynamic fission/fusion events (38, 39) lead to devastating neurological disorders and neurodegeneration.

To identify molecules required for neuronal mitostasis in axons, we performed an unbiased forward genetic screen for mutants that altered the number or size of mitochondrial in sensory axons in the *Drosophila* adult L1 wing vein in vivo. We identified TSG101, a well-known component of the ESCRT-I complex, as required for maintaining normal mitochondrial numbers and sizes. Although we found Shrb, a component of the ESCRT-III complex, was also required for axonal mitostasis like TSG101, we found no evidence for other components or the ESCRT-I, -II, or -III complexes being involved in regulating mitochondria in axons, even when we used null alleles of key components for each complex. These observations support the notion that TSG101 and Shrb regulate mitochondrial numbers and size in a noncanonical ESCRT pathway.

Other components of the ESCRT complexes have recently been linked to mitophagy or autophagy in cultured cells: CHMP2A/Vps2 of ESCRT-III was found to promote mitophagy by mediating phagophore sealing during autophagy, and Snf8/Lsn of ESCRT-II was discovered important in autophagy-independent but endosome-dependent mitochondrial clearance (14–16). However, we found that KO of either of these genes, or full blockade of Parkin/Pink1 mitophagy or autophagy, failed to recapitulate *tsg101*-mutant phenotype or alter mitochondrial numbers or distribution in axons. Live cell imaging of lysosomes reveled their accumulation within the axon, which may occur through the disinhibition of TFEB resulting in their biogenesis. Loss of TSG101 caused an increased proportion of stationary lysosomes in close proximity to mitochondria without subsequent sequestration, since overall mitophagy

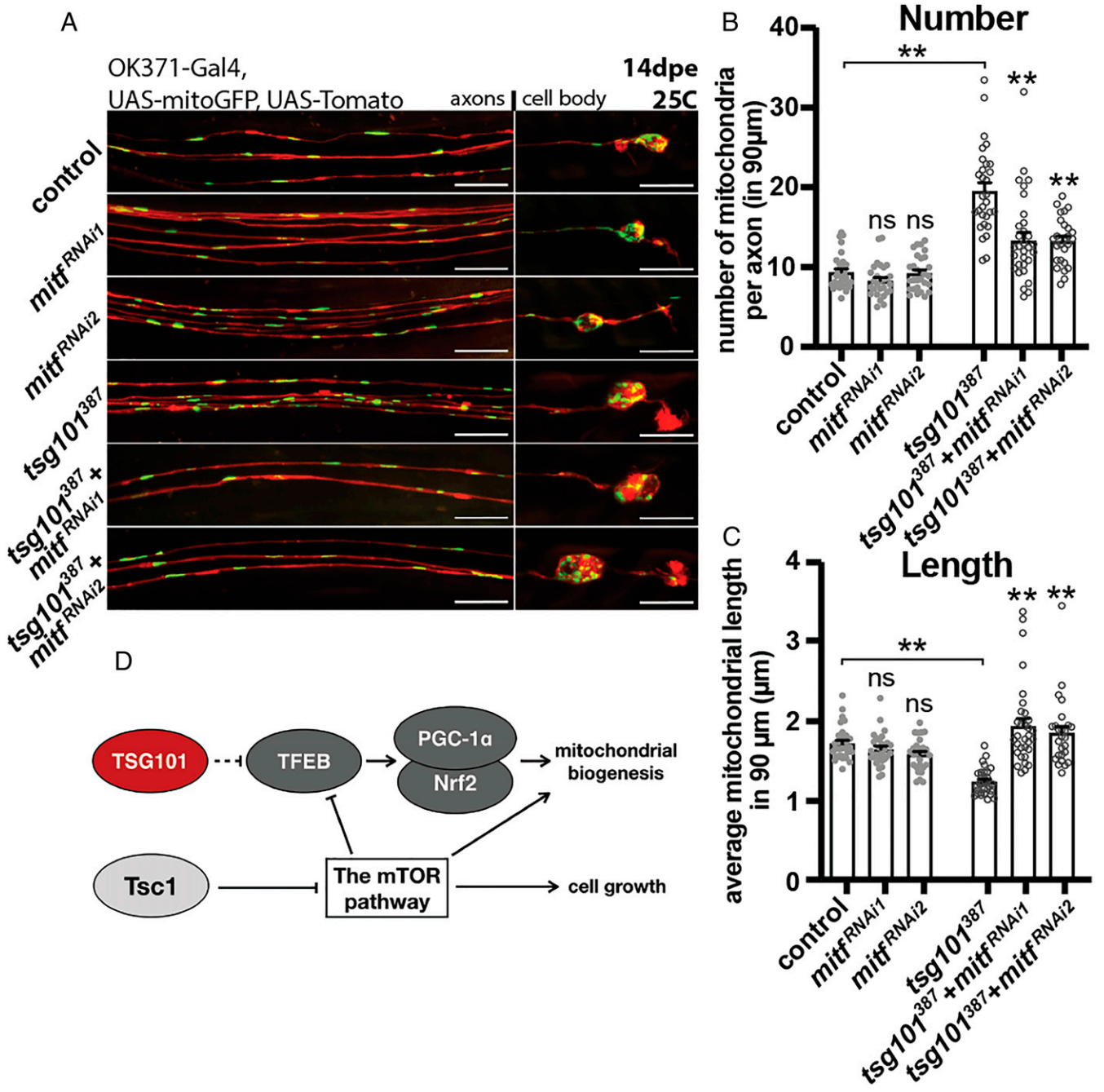

Fig. 5. TFEB (*mitf*) is downstream of TSG101 in mitochondrial regulation. (*A*–*C*) Homozygous mutant neurons were generated and labeled using the same approach as in the previous figure. Two independent RNAi were used to knock down TFEB (*mitf*), and both of them successfully rescued TSG101-mutant phenotype. The result is quantified in *B* and *C* and analyzed via two-way ANOVA. $n \geq 30$. Error bar: SEM. $^{**}P < 0.01$. (Scale bar, 10 μm.) (*D*) A schematic model shows the genetic pathway of TSG101-controlled mitochondrial biogenesis and its relation with the mTOR pathway. In axons mutant for TSG101, TFEB-dependent mitochondrial biogenesis is activated, which requires PGC-1α and Nrf2. As studies have shown that mTOR pathway suppresses TFEB activity and activates mitochondrial biogenesis through transcription factor other than Nrf2, TSG101-controlled mitochondrial biogenesis is parallel to the mTOR pathway.

levels were reduced, indicating deficits in trafficking of mitochondria to lysosomes. It is also possible that accumulation of late endosomes/lysosomes in close proximity may contribute to mitochondrial biogenesis, by serving as translation hubs for mitochondrial encoded proteins, as previously reported (40). Although mitophagy is critical for mitochondrial turnover in many settings, these mechanisms have been studied primarily in the context of cellular stress (e.g., perturbation of mitochondrial membrane potential), while we are examining turnover in wild-type axons in vivo, which might account for some differences in the genetic pathways deployed. Indeed, others have also found that loss of Pink1 or Parkin does not alter axonal mitochondria significantly in vivo (12, 19, 21). We interpret our findings to indicate that at least one component of the ESCRT complex, TSG101, may function in mitophagy regulation under chronic stress yet under normal physiological conditions functions instead as a negative regulator of mitochondrial biogenesis.

Turnover of mitochondria appears to happen in *Drosophila* sensory neuron axons, given that we find small vesicles in axons

consistent with the mito-QC shifting into an acidified compartment. These may be MDVs that are normally shed in control animals and turned over through lysosomal-dependent mechanisms to maintain a functional mitochondria pool in axons. The mechanisms by which turnover occurs in axons is unclear, since loss of Pink1, Parkin, or full blockade of autophagy did not alter mitochondrial numbers in axons. Our data likely indicates that another lysosome-mediated pathway selectively targets MDVs for turnover. Whatever the pathway, it appears sensitive to loss of TSG101: in *tsg101* mutants we found a near complete blockade of turnover of mitochondrial components based on mito-QC dynamics.

In the context of mature axons, how TSG101 and Shrb regulate mitochondrial numbers through regulation of biogenesis is an interesting question. Loss of TSG101 resulted in increased numbers of smaller mitochondria, and multiple measurements of mitochondrial physiology, including sensors of redox status and ATP levels in axons, suggested these mitochondria had less oxidative species and heightened OXPHOS than in controls. These features suggest that TSG101-mutant axons have shifted toward increased mitochondrial biogenesis and therefore argue that TSG101 normally functions in axons to constitutively suppress mitochondrial biogenesis. It would be interesting to see if loss of TSG101 also enhances mitochondrial membrane potential in future studies. TSG101 may regulate signaling back to the nucleus to inhibit activation of the nuclear transcriptional program mediated by PGC-1α, Nrf2, and TFEB, which are key regulators of nuclear mitochondrial genes (41). Interestingly, previous work has shown that TFEB is held on lysosomes when it is not active, and it is released and translocates to the nucleus for transcription upon deactivation of the mTOR pathway (42). It is therefore possible that TSG101 might control TFEB translocation in a similar fashion. TFEB activation is also tightly linked with lysosomal biogenesis and may therefore explain enhanced lysosomal numbers and TSG101-mutant neurons.

Changes in mitochondria occur in *Drosophila* axons with aging. In wild-type animals, mitochondrial numbers remain fairly constant, but average mitochondrial length slowly increases with age. We found that *tsg101*-mutant phenotype manifested as early as 1 dpe and that mitochondrial numbers continued to increase at later time points. Interestingly, mitochondrial length in TSG101 mutants remained short even at late time points, in contrast to wild type where an age-dependent increase was observed. We found that mitochondrial number and size in TSG101 knockdown conditions could be rescued by KO of Drp1, which is consistent with the notion that the final step of mitochondrial biogenesis requires fission (43). Strangely, we also found that elevated mitochondrial numbers in *TSG101*-null clones could be rescued by knockdown of Marf, which should enhance fusion. That manipulating fusion can rescue mutant phenotypes seems counterintuitive and requires further explanation. We note that PGC-1α can activate Mfn2 (Marf homolog) in mammalian cells (44, 45), and to expand to a sizable number of mitochondria (i.e., mitochondrial biogenesis), mitochondrial fusion needs to happen in order to grow mitochondria in size before fission initiates, severing and generating mitochondria from the existing ones. Certainly, overexpression of PCG-1α has also been found to increase the phosphorylation of Drp1 to enhance fusion (46). In the TSG101-KO and Marf knockdown condition, mitochondrial fusion is blocked, and fission is no longer required, hence the inhibition of TSG101-dependent growth in mitochondrial number. How high levels of fission and fusion coordinate with each other to expand a mitochondrial pool in a developing neuron is an interesting and important question for future studies. There is also a possibility that manipulating fusion/fission dynamics can feed back and change how PGC-1α signals downstream of TSG101. Understanding how this feedback mechanism might work is potentially important and requires further investigation.

Our data show that loss of TSG101 causes age-dependent neurodegeneration that occurs independently to changes in mitochondrial dynamics. Prior to cell death, axons are swollen and dysmorphic, recapitulating spongiform phenotypes observed in MGRN1 KO mice (47, 48), associated with loss of TSG101. Genetic blockade of either apoptosis or Wallerian degeneration did not prevent such neurodegeneration, indicating a unique form of cell death, warranting further investigation. Spongiform-like degeneration could be the direct consequence of the accumulation of endosomes or loss of the receptor cargos they contain.

Blocking many key components of the mitophagy pathway did not cause detrimental effects to the axons or their mitochondria, regardless of animal age. This complements the emerging findings that Pink1/Parkin-dependent mitophagy is dispensable in mature neurons under normal physiological conditions (12, 19) and may be protein selective (49). Pink1/Parkin may only be required for mitophagy under scenarios of acute oxidative stress, such as that caused by toxins and rapid depolarization, a context in which Pink1/Parkin–Optineurin signaling is often studied (50–52). It is also interesting to note that blockade of autophagy, and hence all known forms of mitophagy, also had no effect on mitochondria number in axons; however, its blockade did dramatically alter mitochondria in the cell bodies, arguing that mitochondrial regulatory mechanisms in the axon versus cell body are genetically distinct. Genetic evidence has recently linked endosomal trafficking and ubiquitin to long axon maintenance and disease, and the compartmentalization of such processes requires further investigation (53).

To the extent of our knowledge, where biogenesis happens in neurons (i.e., in the axon versus the cell body) is an open question. BrdU labeling studies in isolated chick neurons support the notion that at least in vitro mitochondrial biogenesis can occur in axons (43) and could be triggered by oxidative stress (54), and it seems likely that biogenesis happens in axons in vivo, especially in very long axons that cannot as easily derive such support from the soma. Mitochondrial numbers or position may also meaningfully regulate neurophysiology. Intriguingly, loss of Syntaphilin, a molecule that anchors mitochondria to the cytoskeleton, leads to widespread mitochondrial motility in neurites. Enhanced mitochondrial motility correlated with increased pulse-to-pulse variability in synaptic strength properties, while anchoring mitochondria reduced variability (55). The primary effect of these synaptic changes were found to occur through local modulation of ATP levels (55), which we also observed in *tsg101*-mutant axons. An exciting next question is whether axon-specific regulation of mitochondrial biogenesis or clearance can also provide an additional mechanism to contribute to cell-specific plasticity in circuits.

Materials and Methods

***Drosophila* Strains.** *Drosophila* strains for mutagenesis and MARCM clone generation were as follows: *OK371-Gal4*, *10× UAS-IVS-myr::tdTomato*, *5× UAS-mito::GFP, asense-FLP2e*; *tub-Gal80*, *FRT2A* (females) and *OK371-Gal4*, *10× UAS-IVS-myr::tdTomato*; *FRT2A*, *FRT82B* (males). Fly lines used for MARCM clone generation in epistatic analyses or general experimental procedures are the following: *OK371-Gal4*, *nSyb-Gal4*, *FRT19A*, *FRT40A*, *FRT2A*, *FRT80B*, *FRT82B*, *asense-FLP^{2c}*, *asense-FLP^{2e}*, *asense-FLP^{3b}*, *hs-FLP^{122}*, *tub-Gal80*, *10× UAS-IVS-myr::tdTomato*, *5× UAS-mito::GFP*, *5× UAS-mito::tdTomato*, and *5× UAS-lamp1::GFP*. MARCM tools and resourses were generated by ref. (56). The following null mutant alleles, overexpression constructs, and commercially available RNAi lines were used in epistasis or general experiments: *tsg101^{942}* (Bloomington Drosophila Stock Center [BDSC]: 63105), *lsn^{ss6}* (BDSC: 39631), *vps2^{pp6}* (BDSC: 39630), *ALiX^{LL05494}* (Kyoto: 140993), *shrb^{G5}* (BDSC: 39635), *shrb^{O3}* (BDSC: 39623), *mop^{T612}* (BDSC: 63117), *parkin$^{\Delta 21}$* (BDSC: 51652), *Pink1^{5}* (BDSC: 51649), *drp1^{1}* (BDSC: 24885), *atg6$^{\Delta 1}$* (57), BAC$_{CH322\text{-}97B15}$ (covering *tsg101*; GenetiVision) (Stock ID: P9-D10), *UAS-atg1.K38Q* dominant negative (58), *UAS-hUCP2* (59), *5× UAS-tsg101^{RNAi}* (BDSC: 35710), *5× UAS-tsc1^{RNAi}* (BDSC: 54034), *5× UAS-shrb^{RNAi}* (BDSC: 38305), *5× UAS-marf^{RNAi}* (BDSC: 55189), *5× UAS-srl^{RNAi}* (Vienna Drosophila Resource Center [VDRC]: 330271), *5× UAS-srl^{RNAi}* (VDRC: 103355), *5× UAS-cnc^{RNAi}* (BDSC: 40854), *5× UAS-cnc^{RNAi}* (VDRC: 37673), *5× UAS-mitf^{RNAi}* (BDSC: 44561), *5× UAS-mitf^{RNAi}* (VDRC: 109184), *5× UAS-Stam^{RNAi}*

(BDSC: 27487, BDSC: 35016, VDRC: 22497, and VDRC: 330248), 5× *UAS-Hrs*^{RNAi} (BDSC: 28026, BDSC: 33900, BDSC: 34086, and VDRC: 330597), 5× *UAS-vps37*^{RNAi} (BDSC: 38304, VDRC: 39885, VDRC: 104530, BDSC: 44010, BDSC: 60416, and VDRC: 330553), 5× *UAS-vps28*^{RNAi} (VDRC: 31894, VDRC: 31895), 5× *UAS-vps36*^{RNAi} (BDSC: 38286, VDRC: 16846, VDRC: 16847, and VDRC: 107417), 5× *UAS-lsn*^{RNAi} (BDSC: 38289, VDRC: 21658, and VDRC:110350), 5× *UAS-vps25*^{RNAi} (BDSC: 26286, BDSC: 54831, VDRC: 38821, and VDRC: 108105), 5× *UAS-vps20*^{RNAi} (BDSC: 40894, VDRC: 26387, VDRC: 26388, and VDRC: 103944), 5× *UAS-vps20*^{RNAi} (BDSC: 40894, VDRC: 26387, VDRC: 26388, and VDRC: 103944), 5× *UAS-vps2*^{RNAi} (BDSC: 38995 and VDRC: 24869), 5× *UAS-vps4*^{RNAi} (BDSC: 31751, VDRC: 35125, VDRC: 35126, and VDRC: 105977), 5× *UAS-Chmp1*^{RNAi} (BDSC: 28906, BDSC: 33928, and VDRC: 1788), 5× *UAS-ALiX*^{RNAi} (BDSC: 33417, BDSC: 50904, VDRC: 32047, and VDRC: 32049), 5× *UAS-usp8*^{RNAi} (BDSC: 38982, BDSC: 39022, and VDRC: 330131), and 5× *UAS-mop*^{RNAi} (BDSC: 28522, BDSC: 32916, BDSC: 34085, VDRC: 14173, and VDRC: 104860). The following redox-sensing GFPs were used to assess mitochondrial health: 5× *UAS-mito-Grx1-roGFP2* (GSSG-sensing, BDSC: 67664) and 5× *UAS-mito-roGFP2-Orp1* (H_2O_2-sensing, BDSC: 67667). *UAS-mito-QC* [gifted by Whitworth Lab, University of Cambridge, Cambridge, UK (19)] was used to visualize mitochondrial turnover events. *UAS-ATPsnFR* (this work) was utilized for measuring the ATP level in neurons. Due to no phenotypic difference between sexes, adult flies of both sexes were used throughout all the experiments. Wings with obvious damage were not used for imaging or incorporated into datasets. Mutant experiments were conducted at 25 °C and upstream activation sequence (UAS)-driven RNAi/transgene overexpression experiments conducted at 29 °C.

MARCM Clone Induction and In Vivo Mutagenesis Screen for Changes in Mitochondrial Morphology. Induction of MARCM clones in *Drosophila* wings was described in our previous work (17), which was adapted from an axon destruction screen (56). The screen started off by starving male flies for 8 h followed by feeding mutagen EMS (Sigma-Aldrich catalog no. M0880) for 12 h (25 mM EMS in 1% sucrose). The males were kept in fresh vials to recover for another 12 h before mating with females. The F1 progeny, aged 7 dpe at 25 °C were checked by clipping off one wing per fly, mounting the wings directly in Halocarbon Oil 27 (Sigma-Aldrich catalog no. H8773) on a microscopy slide with coverslip on top, and immediately examining under microscope. Axonal mitochondria (labeled with *mito::GFP*) residing in the L1 vein of each wing were checked for any phenotypic changes. Flies that exhibited phenotypes were saved, bred, outcrossed, and made into stocks for further analysis including deficiency mapping and whole-genome sequencing. For the subsequent experiments, the MARCM clones were induced the same way as in the mutagenesis screen except in the ATPsnFR experiment (Fig. 3 *E* and *F*), in which the MARCM clones were generated via heat shock (37 °C for 1 h and 6 d after mating).

Whole-Genome Sequencing. The nature of gene mutations responsible for mitochondrial phenotypes were identified by next-gen whole-genome sequencing. Genomic DNA was extracted from more than 200 heterozygous adult flies, then sequenced via HiSeq2000 sequencing system (Illumina). Further analysis in order to identify mutations/variants was carried out through the Center for Genome Technology, University of Miami.

Immunocytochemistry. Primary mouse cortical neurons (ThermoFisher A15586) were purchased and plated onto poly-L-lysine-coated coverslips in 12-well plates containing plating medium (MEM with L-glutamine, 10% horse and fetal bovine serum, pen strep, and 25 mM glucose). Plating medium was replaced with Neurobasal medium, B-27 supplement, and GlutaMAX supplement after 24 h, and cells were fed every 3 d. At 12 days in vitro, mouse cortical neurons were washed twice with Dulbecco's phosphate-buffered saline (D-PBS), fixed in 4% paraformaldehyde for 15 min at room temperature (RT), and rinsed three times with D-PBS. Neurons were permeabilized with 0.3% Triton ×100 and blocked in 5% goat serum for 1 h at RT. Cells were washed three times in D-PBS and incubated overnight at 4 °C with the primary antibody. The following primaries were used: anti-TSG101G (rabbit, Abcam ab125011, 1:50), anti-TOMM20 (mouse, Abcam ab56783, 1:100), and anti-EEA1 (mouse, Santa Cruz sc-137130, 1:100). Cells were washed and incubated with donkey Alexa-488–conjugated anti-rabbit (Abcam a21206, 1:1,000) and goat Alexa-568–conjugated anti-mouse (Abcam, ab175473, 1:1,000) secondary antibodies for 1 h at RT. Cells were washed three times with D-PBS, counterstained with Hoechst for 30 min at RT, rinsed, and mounted with Prolong Gold antifade solution.

Microscopy and Data Analysis. Fly images were acquired by Zeiss spinning disk confocal microscope alongside its proprietary Zen Blue software. Images were processed in Zen Blue and Fiji (version 2.0). Fiji was used to quantify mitochondrial number, mitochondrial length, cell body size, and fluorescence intensities. Cortical neuron images were acquired by Leica TCS SP8 scanning confocal microscope and LAS X software. Images were processed in Fiji (version 2.0). All statistical analyses were conducted in Graph Pad Prism 8. More information such as statistical methods and number of animals can be found in Figs. 1–5.

Data Availability. All study data are included in the article and/or *SI Appendix*.

ACKNOWLEDGMENTS. We thank the Looger laboratory in the Janelia Research Campus for providing the backbone plasmids for making the ATPsnFR transgenic fly, the Whitworth laboratory at University of Cambridge for the mito-QC transgenic fly, Lukas Neukomm for MARCM flies, the Baehrecke laboratory at the University of Massachusetts Medical School for the *atg6* KO fly, and Bloomington Drosophila Stock Center, Kyoto Stock Center, and Vienna Drosophila Resource Center for the rest of the reagents. We also thank Dr. Kelly Monk, Dr. Philip Copenhaver, Dr. Alex Nechiporuk, and Dr. Gail Mandel at the Vollum Institute of Oregon Health & Science University for critical feedback. This work was funded by NIH R21 (NS098364 to M.R.F. and G.A.S.), Medical Research Council Momentum Award (MC_PC_16030/1 to G.A.S.), NIH RO1 NS059991 (to M.R.F.), the UK Dementia Research Institute, Cardiff University, and Oregon Health & Science University.

1. S. M. Han, H. S. Baig, M. Hammarlund, Mitochondria localize to injured axons to support regeneration. *Neuron* **92**, 1308–1323 (2016).
2. R. L. Rawson *et al*., Axons degenerate in the absence of mitochondria in C. elegans. *Curr. Biol.* **24**, 760–765 (2014).
3. V. L. Hewitt, A. J. Whitworth, "Mechanisms of Parkinson's disease" in *Current Topics in Developmental Biology*, Pick L., Ed. (Elsevier, 2017), pp. 173–200.
4. M. Jodeiri Farshbaf, K. Ghaedi, Huntington's disease and mitochondria. *Neurotox. Res.* **32**, 518–529 (2017).
5. J.-S. Park, R. L. Davis, C. M. Sue, Mitochondrial dysfunction in Parkinson's disease: New mechanistic insights and therapeutic perspectives. *Curr. Neurol. Neurosci. Rep.* **18**, 21 (2018).
6. N. Salvadores, M. Sanhueza, P. Manque, F. A. Court, Axonal degeneration during aging and its functional role in neurodegenerative disorders. *Front. Neurosci.* **11**, 451 (2017).
7. J. E. Dominy, P. Puigserver, Mitochondrial biogenesis through activation of nuclear signaling proteins. *Cold Spring Harb. Perspect. Biol.* **5**, a015008 (2013).
8. Y. Chen, G. W. Dorn, II, PINK1-phosphorylated mitofusin 2 is a Parkin receptor for culling damaged mitochondria. *Science* **340**, 471–475 (2013).
9. D. Narendra, A. Tanaka, D.-F. Suen, R. J. Youle, Parkin is recruited selectively to impaired mitochondria and promotes their autophagy. *J. Cell Biol.* **183**, 795–803 (2008).
10. D. P. Narendra *et al*., PINK1 is selectively stabilized on impaired mitochondria to activate Parkin. *PLoS Biol.* **8**, e1000298 (2010).
11. E. S. Vincow *et al*., The PINK1-Parkin pathway promotes both mitophagy and selective respiratory chain turnover in vivo. *Proc. Natl. Acad. Sci. U.S.A.* **110**, 6400–6405 (2013).
12. H. Sung, L. C. Tandarich, K. Nguyen, P. J. Hollenbeck, Compartmentalized regulation of parkin-mediated mitochondrial quality control in the Drosophila nervous system in vivo. *J. Neurosci.* **36**, 7375–7391 (2016).
13. C. S. Evans, E. L. F. Holzbaur, Quality control in neurons: Mitophagy and other selective autophagy mechanisms. *J. Mol. Biol.* **432**, 240–260 (2020).
14. Y. Takahashi *et al*., An autophagy assay reveals the ESCRT-III component CHMP2A as a regulator of phagophore closure. *Nat. Commun.* **9**, 2855 (2018).
15. Y. Zhen *et al*., ESCRT-mediated phagophore sealing during mitophagy. *Autophagy* **16**, 826–841 (2019).
16. B. C. Hammerling *et al*., A Rab5 endosomal pathway mediates Parkin-dependent mitochondrial clearance. *Nat. Commun.* **8**, 14050 (2017).
17. G. A. Smith *et al*., Glutathione S-transferase regulates mitochondrial populations in axons through increased glutathione oxidation. *Neuron* **103**, 52–65.e6 (2019).
18. T. Lee, L. Luo, Mosaic analysis with a repressible cell marker for studies of gene function in neuronal morphogenesis. *Neuron* **22**, 451–461 (1999).
19. J. J. Lee *et al*., Basal mitophagy is widespread in Drosophila but minimally affected by loss of Pink1 or parkin. *J. Cell Biol.* **217**, 1613–1622 (2018).
20. T. G. McWilliams *et al*., *mito*-QC illuminates mitophagy and mitochondrial architecture in vivo. *J. Cell Biol.* **214**, 333–345 (2016).
21. T. G. McWilliams *et al*., Basal mitophagy occurs independently of PINK1 in mouse tissues of high metabolic demand. *Cell Metab.* **27**, 439–449.e5 (2018).
22. S. C. Albrecht, A. G. Barata, J. Grosshans, A. A. Teleman, T. P. Dick, In vivo mapping of hydrogen peroxide and oxidized glutathione reveals chemical and regional specificity of redox homeostasis. *Cell Metab.* **14**, 819–829 (2011).
23. M. A. Lobas *et al*., A genetically encoded single-wavelength sensor for imaging cytosolic and cell surface ATP. *Nat. Commun.* **10**, 711 (2019).
24. C. Fleury *et al*., Uncoupling protein-2: A novel gene linked to obesity and hyperinsulinemia. *Nat. Genet.* **15**, 269–272 (1997).
25. G. Mansueto *et al*., Transcription factor EB controls metabolic flexibility during exercise. *Cell Metab.* **25**, 182–196 (2017).

26. C. Settembre *et al*., TFEB controls cellular lipid metabolism through a starvation-induced autoregulatory loop. *Nat. Cell Biol.* **15**, 647–658 (2013).
27. J. T. Cunningham *et al*., mTOR controls mitochondrial oxidative function through a YY1-PGC-1α transcriptional complex. *Nature* **450**, 736–740 (2007).
28. J. A. Martina, Y. Chen, M. Gucek, R. Puertollano, MTORC1 functions as a transcriptional regulator of autophagy by preventing nuclear transport of TFEB. *Autophagy* **8**, 903–914 (2012).
29. G. Napolitano *et al*., mTOR-dependent phosphorylation controls TFEB nuclear export. *Nat. Commun.* **9**, 3312 (2018).
30. C. Chen *et al*., TSC-mTOR maintains quiescence and function of hematopoietic stem cells by repressing mitochondrial biogenesis and reactive oxygen species. *J. Exp. Med.* **205**, 2397–2408 (2008).
31. M. A. Avery *et al*., WldS prevents axon degeneration through increased mitochondrial flux and enhanced mitochondrial Ca2+ buffering. *Curr. Biol.* **22**, 596–600 (2012).
32. B. A. Hay, T. Wolff, G. M. Rubin, Expression of baculovirus P35 prevents cell death in Drosophila. *Development* **120**, 2121–2129 (1994).
33. M. Ollmann *et al*., Drosophila p53 is a structural and functional homolog of the tumor suppressor p53. *Cell* **101**, 91–101 (2000).
34. T. Misgeld, T. L. Schwarz, Mitostasis in neurons: Maintaining mitochondria in an extended cellular architecture. *Neuron* **96**, 651–666 (2017).
35. R. F. Roberts, M. Y. Tang, E. A. Fon, T. M. Durcan, Defending the mitochondria: The pathways of mitophagy and mitochondrial-derived vesicles. *Int. J. Biochem. Cell Biol.* **79**, 427–436 (2016).
36. E. Shlevkov, T. L. Schwarz, Have you seen? For parkin, it's not all or nothing. *EMBO J.* **33**, 277–279 (2014).
37. M. T. Lin, M. F. Beal, Mitochondrial dysfunction and oxidative stress in neurodegenerative diseases. *Nature* **443**, 787–795 (2006).
38. A. Olichon *et al*., Mitochondrial dynamics and disease, OPA1. *Biochim. Biophys. Acta* **1763**, 500–509 (2006).
39. S. Züchner *et al*., Mutations in the mitochondrial GTPase mitofusin 2 cause charcot-marie-tooth neuropathy type 2A. *Nat. Genet.* **36**, 449–451 (2004).
40. J.-M. Cioni *et al*., Late endosomes act as mRNA translation platforms and sustain mitochondria in axons. *Cell* **176**, 56–72.e15 (2019).
41. D. P. Kelly, R. C. Scarpulla, Transcriptional regulatory circuits controlling mitochondrial biogenesis and function. *Genes Dev.* **18**, 357–368 (2004).
42. C. Settembre *et al*., A lysosome-to-nucleus signalling mechanism senses and regulates the lysosome via mTOR and TFEB. *EMBO J.* **31**, 1095–1108 (2012).
43. M. Amiri, P. J. Hollenbeck, Mitochondrial biogenesis in the axons of vertebrate peripheral neurons. *Dev. Neurobiol.* **68**, 1348–1361 (2008).
44. R. Cartoni *et al*., Mitofusins 1/2 and ERRα expression are increased in human skeletal muscle after physical exercise: Mitofusins 1/2 and ERRα expression in skeletal muscle. *J. Physiol.* **567**, 349–358 (2005).
45. F. X. Soriano *et al*., Evidence for a mitochondrial regulatory pathway defined by peroxisome proliferator-activated receptor-gamma coactivator-1 alpha, estrogen-related receptor-alpha, and mitofusin 2. *Diabetes* **55**, 1783–1791 (2006).
46. K. Peng *et al*., The interaction of mitochondrial biogenesis and fission/fusion mediated by PGC-1α regulates rotenone-induced dopaminergic neurotoxicity. *Mol. Neurobiol.* **54**, 3783–3797 (2017).
47. L. He *et al*., Spongiform degeneration in mahoganoid mutant mice. *Science* **299**, 710–712 (2003).
48. J. Jiao *et al*., Abnormal regulation of TSG101 in mice with spongiform neurodegeneration. *Biochim. Biophys. Acta* **1792**, 1027–1035 (2009).
49. E. S. Vincow *et al*., Autophagy accounts for approximately one-third of mitochondrial protein turnover and is protein selective. *Autophagy* **15**, 1592–1605 (2019).
50. A. M. Pickrell *et al*., Endogenous parkin preserves dopaminergic substantia nigral neurons following mitochondrial DNA mutagenic stress. *Neuron* **87**, 371–381 (2015).
51. C. S. Evans, E. L. Holzbaur, Degradation of engulfed mitochondria is rate-limiting in Optineurin-mediated mitophagy in neurons. *eLife* **9**, e50260 (2020).
52. C. S. Evans, E. L. F. Holzbaur, Lysosomal degradation of depolarized mitochondria is rate-limiting in OPTN-dependent neuronal mitophagy. *Autophagy* **16**, 962–964 (2020).
53. M. A. Farazi Fard *et al*., Truncating mutations in UBAP1 cause hereditary spastic paraplegia. *Am. J. Hum. Genet.* **104**, 767–773 (2019).
54. V. S. Van Laar *et al*., Evidence for compartmentalized axonal mitochondrial biogenesis: Mitochondrial DNA replication increases in distal axons as an early response to Parkinson's disease-relevant stress. *J. Neurosci.* **38**, 7505–7515 (2018).
55. T. Sun, H. Qiao, P.-Y. Pan, Y. Chen, Z.-H. Sheng, Motile axonal mitochondria contribute to the variability of presynaptic strength. *Cell Rep.* **4**, 413–419 (2013).
56. L. J. Neukomm, T. C. Burdett, M. A. Gonzalez, S. Züchner, M. R. Freeman, Rapid in vivo forward genetic approach for identifying axon death genes in *Drosophila*. *Proc. Natl. Acad. Sci. U.S.A.* **111**, 9965–9970 (2014).
57. S. Zhao, T. M. Fortier, E. H. Baehrecke, Autophagy promotes tumor-like stem cell niche occupancy. *Curr. Biol.* **28**, 3056–3064.e3 (2018).
58. D. L. Berry, E. H. Baehrecke, Growth arrest and autophagy are required for salivary gland cell degradation in Drosophila. *Cell* **131**, 1137–48 (2007).
59. Y.-W. C. Fridell, A. Sánchez-Blanco, B. A. Silvia, S. L. Helfand, Targeted expression of the human uncoupling protein 2 (hUCP2) to adult neurons extends life span in the fly. *Cell Metab.* **1**, 145–52 (2005).